ULTRA-HIGH PERFORMANCE FIBRE-REINFORCED CEMENTITIOUS COMPOSITE WITH STEEL MICROFIBRES FUNCTIONALIZED WITH SILANE

Cézar Augusto Casagrande[1*]; Sergio Henrique Pialarissi Cavalaro[2]; Wellington Longuini Repette[1].

[1] Department of Civil Engineering (ECV), Federal University of Santa Catarina (UFSC), João Pio Duarte Silva s/n, Córrego Grande, CEP 88040-900 Florianópolis, Santa Catarina, Brazil

[2] School of Architecture, Building and Civil Engineering, Loughborough University Leicestershire, LE11 3TU, UK.

*Corresponding author: cezar.acasa@gmail.com (C.A. Casagrande).

HIGHLIGHTS:

- Silane film of TEOS is formed over the fibre after functionalization;
- Increase of silane content in functionalization leads to higher pullout bond strength;
- Functionalization with TEOS enhance fibre–matrix interfacial properties;
- The Si/Ca ratio in the fibre-matrix interface is increased when the TEOS functionalization is applied;

ABSTRACT

This paper explores the effect of fibre functionalization with tetraethoxysilane (TEOS) in the microstructure and mechanical property of ultra-high performance cement composites with steel fibres. Fibres treated with three concentrations of TEOS were evaluated by pullout tests and SEM/EDS analysis. Mixes with treated fibres showed up to 35.6% increase in bond strength and up to 49.5% reduction in the crack opening at the peak pullout load in comparison with

reference mixes containing untreated fibres. The Si/Ca ratios in the fibre-matrix transition zone increases with the increment of the concentration of TEOS in the treatment of the fibre. This indicates an increase of C-S-H at the interface that justifies the enhanced mechanical performance.

KEYWORDS: Silane, fibre pullout, functionalization, interface adhesion, UHPFRC.

1 INTRODUCTION

Introduced in the 80's, Ultra-High Performance Fibre Reinforced Concrete (UHPFRC) [1,2] has very high compressive strength (more than 150 MPa at 28 days [3,4]) and enhanced durability [5]. This is achieved by combining high content of binders, low water-to-binder ratios (typically smaller than 0.20 by weight) and ultrafine mineral admixtures. In most structural applications, mixes incorporate straight metallic microfibres to compensate for the brittle behaviour of the cementitious matrix and to achieve higher ductility and toughness in tension [6,7].

Pullout tests of UHPFRC, performed in specimens with aligned straight steel fibres embedded in cementitious concrete matrix, reveal a three-stage mechanical response [8–11]. An elastic stage takes place for small displacements as fibre and matrix show compatible deformation and the integrity of the fibre-matrix interface is maintained. As the load increases, tangential stresses in the fibre-matrix interface induce micro-cracks along the length of the fibre, initiating the debonding stage. Once the tangential stress reaches the bond strength along a critical length, the integrity of the interface is fully compromised and the strain compatibility between fibre and matrix cease to exist. The sliding stage follows, characterized by the relative displacement between fibre and matrix. The restriction to this movement is the result of friction at the fibre-matrix interface.

Since the tensile failure of UHPFRC is governed by the bond between fibre and matrix, attempts to enhance the mechanical performance of the material in tension often focus on

improving the interfacial properties through modifications of the matrix composition or of the fibre geometry [12–14]. Few studies have addressed this issue by means of surface treatments applied to the surface of metallic fibres, prior to their mixing with concrete.

In several industrial applications, silane films are used as surface coatings to improve corrosion resistance [15,16] and as a primer to improve the adhesion of other polymeric coatings to metal plates [17,18]. Silanes are molecules of general formula $R'_y(CH_2)_nSi(OR)_{4-y}$, in which R' is an organofunctional group and R is a hydrolysable alkoxy group [19]. Studies with silane coupling agents showed the possibility of producing sheets of hybrid calcium silicate hydrate from the reaction of hydrolysed silanes in calcium hydroxide solution at room temperature [20–22]. Other studies revealed the potential use of silanes to improve properties in cement-based materials, such as workability or durability [23–28].

Research on modification of fibre surface with silanes to improve the performance of interfaces with cement-based matrices is still limited. [29] and [30] evaluated the mechanical properties of non-metallic fibres treated with silane and embedded in conventional cement matrixes. Pullout tests indicated an increase of up to 150% in the average bond strength and of up to 300% in the toughness. Similarly, [31] performed surface modification of polymeric fibres with silane for reinforcement of concrete. The authors found that the increase of mechanical properties resulted from the formation of high amount of calcium silicates hydrates (C-S-H) at the surface of the fibre.

However, the application of silane surface treatments to improve the performance of metallic fibres in UHPFRC is still unexplored. The objective of this study is to investigate the influence of steel fibres functionalization with silane on the pullout behaviour and on the characteristics of the fibre-matrix interface in UHPFRC.

2 EXPERIMENTAL PROGRAM

2.1 FIBRE TREATMENT

Brass covered straight steel microfibre, with 13 mm of length, 0.16 mm of diameter and tensile strength of 2000 MPa was used in this study. This fibre has been extensively used in UHPFRC. The surface treatment used tetraethoxysilane ($C_8H_{20}O_4Si$) – a silane also known as TEOS with purity higher than 98% and specific gravity of 0.9935 g/cm³. TEOS is among the most commonly used silanes in industrial functionalization of metals due to its controllable hydrolysis velocity and high degree of crosslink [32].

For effective functionalization with TEOS, all four methoxy groups have to be hydrolysed to release hydroxyls radicals (silanol) able to react with the base surfaces (metallic surface, in this case). Fig. 1 shows the representation of the procedure of hydrolyse of the TEOS, based on [24,33,34]. Since TEOS is not miscible in water, a 1:1 solution by volume of ethanol (C_2H_6O with purity higher than 96%) in water was used to disperse the silane. Then, acetic acid was added to ensure a solution with pH of 5±0.2. After that, the solution was constantly homogenized in a magnetic stirrer at 25 °C. The optimum hydrolysis time was determined by infrared analysis (FT-IR). The transmittance of the wavenumber in the interval of approximately 960 cm^{-1} indicates the Si-OH (silanol) formation. Lower index at 960 cm^{-1} bands indicates a larger concentration of silanol groups produced by hydrolysis. The lowest wavenumber index was observed after 60 min of hydrolysis.

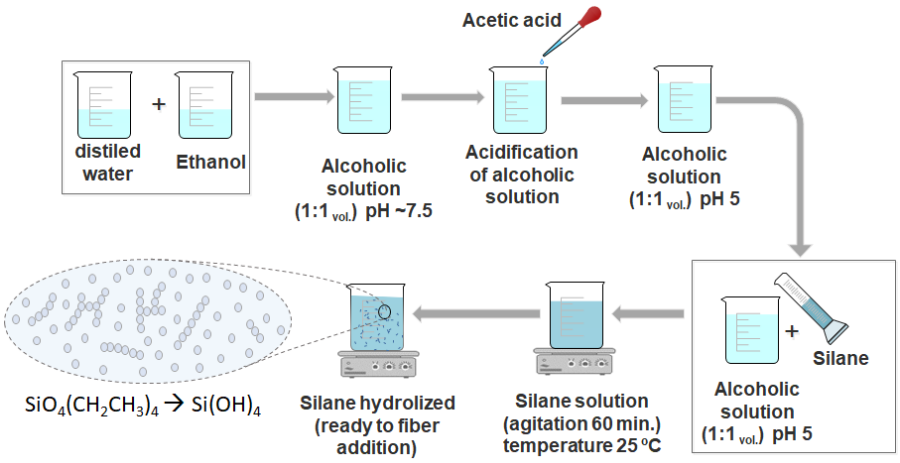

Fig. 1 - Representation of the TEOS hydrolysis procedures

Silane concentrations of 1.0% by volume are typically used for industrial functionalization of metallic plates with amino, ureido and epoxysilanes [35–37]. For the functionalization of synthetic fibres, [29] and [30] used concentrations of 0.5%, 0.75% and 1.0% by volume of vinylsilane. Based on that, solutions with 0.1%, 0.5% and 1.0% of TEOS by volume were prepared in the present study (T_0.1%, T_0.5% and T_1.0%, respectively).

Fig. 2 summarizes the steps for the functionalization of the steel fibres, which was adapted from the work by [33]. Fibres were first submerged during 2 minutes in 1:0.25 solution of acetone (C_3H_6O with purity higher than 96%) in water to remove dust or grease off their surface and, then, dried during 12 hours in a ventilated oven at 100 °C.

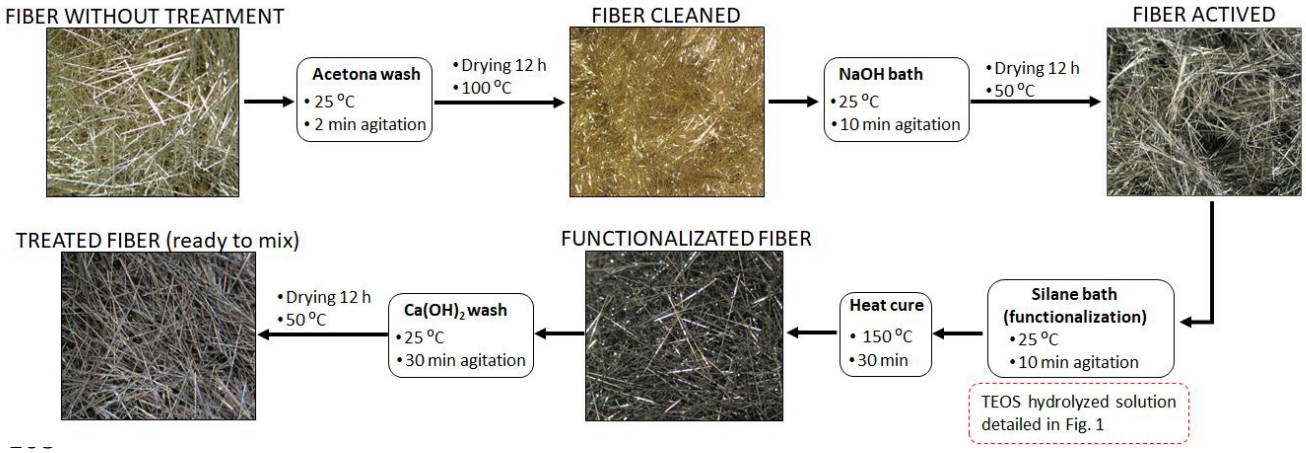

Fig. 2 – Steps of fibre surface treatment

Next, the surface of the fibres was activated by the deposition of hydroxyl groups (OH^-) that might react with TEOS. Fibres were submerged in a 0.625 M aqueous solution of NaOH (97% purity) at 25°C under constant agitation for 10 min, rinsed with distilled water and dried in an oven at 50 °C for 12 hours. At this stage of the process, the surface of the fibres composed of a thin layer of brass oxidizes superficially, resulting in a darker finishing. This surface oxidation does not damage the steel of the fibre or affect the efficiency of the functionalization process. After that, the functionalization of the surface with TEOS was conducted following a sol-gel dip coating process. Fibres were submerged in the solution with the hydrolysed TEOS produced

119 according with Fig. 1, in a proportion of 300 g/L. The components were constantly agitated in a
120 mechanical stirrer during 10 min at 25 °C, rinsed in distilled water and cured for 30 min in an
121 oven at 150 °C.

122 Fibres were then submerged in a 0.1 M aqueous solution of $Ca(OH)_2$ (purity higher than
123 95%), which was agitated for 30 min at 25°C to remove loose TEOS from the surface. The removal
124 of loose TEOS film prevented undesirable change in the composition of UHPFRC and a
125 retardation of the cement setting observed in the presence of loose TEOS film during a
126 preliminary stage of the experimental program. Finally, fibres were rinsed in distilled water and
127 oven dried at 50 °C for 12 h.

128

129 2.2 PREPARATION OF THE COMPOSITE SPECIMENS

130 An initial experimental campaign was conducted to adjust the mix and to assure the
131 desired performance in fresh and hardened states. Table 1 shows the materials and the
132 composition defined used to produce the UHPFRC (defined in accordance with previous studies
133 by [38–40]).

134

135 Table 1 – Components and mix composition of UHPFRC

Materials	Density	Proportion by weight	kg/m³	Apparent volume (%)
Cement CEM I 52.5R	3.11	1.00	939.8	30.21
Fine Sand	2.64	1.21	1140.3	43.19
$CaCO_3$ powder	2.70	0.11	103.4	3.82
Superplasticizer	1.05	0.07	66.2	6.30
Nano-silica	1.13	0.07	67.2	5.92
Mixing water	1.00	0.09	85.8	8.58
Fibres (untreated)	7.95	0.16	155.1	2.00

136

137 The Cement CEM I 52.5R followed the specifications of EN 197-1 [41]. The silica sand had
138 99.5% of SiO_2, a maximum nominal particle size of 0.6 mm and an average particle size of 0.3
139 mm. $CaCO_3$ powder with average particle size of 3.9 μm was used as filler. Nano-silica, in
140 suspension with a solid content of 22% and average particle size of 99.35 nm, was also used. The

141 superplasticizer was a sodium polycarboxylate with a solid content of 25%. The effective water-
142 to-cement ratio (considering the water provided by the components) was approximately 0.20.
143 UHPFRC with the composition from Table 1 had an average flow of 191 mm in accordance with
144 ASTM C1437 [42]. The average compressive strength at 28 days according to the EN 196-1 [43]
145 was 172.4 MPa, with a standard deviation of 6.7 MPa.

146 All mixes were produced with 2% by volume of fibres treated with the silane
147 concentrations described in previous sections (T_0.1%, T_0.5%, and T_1.0%). For comparative
148 purposes, reference mixes with untreated fibres (REF) were also produced.

149 A mixer model with a vertical axis was used. First, all solid materials were homogenized
150 for 3 min. Then, the liquids were added in the following order separated from each other by 1
151 min of mixing: all nano-silica, 50% of the water, 90% of superplasticizer and the remaining
152 liquids. After mixing for 5 min, fibres were slowly added during 5 min. Finally, the UHPFRC was
153 mixed for 5 min more.

154 Then, specimens were cast for the pullout test of multiple fibres, similarly to the described
155 in [10], [14] and [44]. A thin polyethylene plastic sheet with dimensions 40x40x0.5 mm was
156 pierced with evenly spaced holes forming a 5 by 5 grid. Fibres were placed at half of their length,
157 perpendicularly to each hole (Fig. 3.a). The polyethylene sheet was, then, positioned at the
158 central part of a mould with internal dimensions of 40x40x80 mm. This guaranteed a uniform
159 fibre distribution, their perpendicular alignment with the largest dimension of the specimen and
160 a preferential cracking plane during the pullout tests.

161 The UHPFRC was poured on both sides of the thin polyethylene sheet and compacted in
162 accordance with UNE-EN 196-1 [43]. Special care was taken to guarantee a complete filling of
163 the space between fibres, minimizing their displacement or spin. Specimens were demoulded
164 24 hours of casting, remaining in a climatic chamber at 23 °C and relative humidity higher than
165 99% for 28 days. Six specimens per series were produced.
166

2.3 PULL OUT TESTING PROCEDURE

Fig. 3.b shows the setup of the pullout test conducted in a hydraulic press, using a load cell with 5 kN nominal capacity and 0.001 kN resolution. Both ends of the specimens were glued with an epoxy adhesive to the plates of the press. An extensometer was placed with the cracking plane in the middle. Following [10], the test was conducted at a constant displacement rate of 0.3 mm/min controlled by the extensometer. The pullout load (*P*) was registered throughout the test.

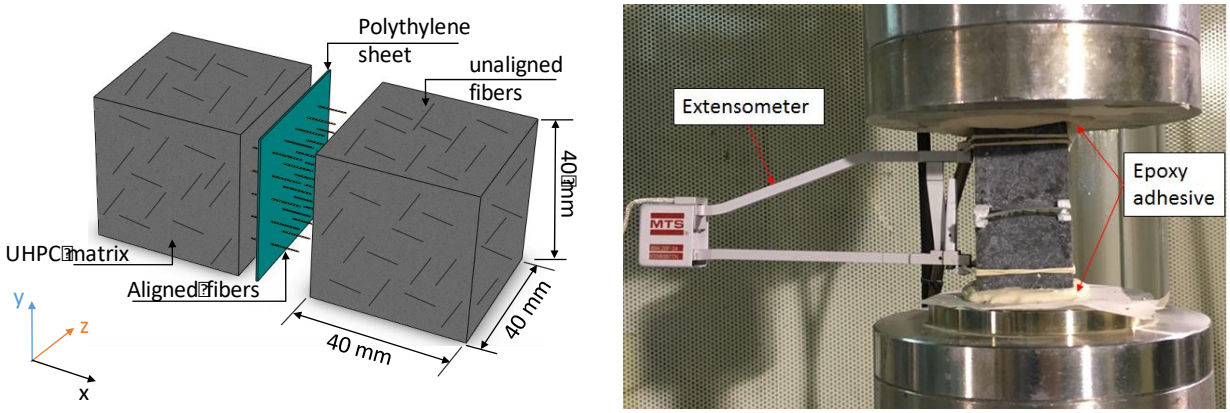

(a) (b)

Fig. 3 - Pullout samples: detailed view of parts of the specimen (a) and pullout test setup (b)

The displacement registered by the extensometer is the summed result of the crack opening and the elastic deformation of the UHPFRC between the points of measurements. Due to the low load reached during the test and the high Young Modulus of the UHPFRC, the displacement induced by the elastic deformation is several orders of magnitude smaller than the sensitivity of the extensometer and may be disregarded. Therefore, the displacement is considered equal to the crack opening (*w*).

As in other studies [10,45,46], the average bond strength (τ_{max}) was calculated according to Eq. (1) that assumes an uniform stress distribution at the fibre-matrix interface. P_{max} is the maximum pullout load, *n* is the number of fibres in the cracked section, *d* is the fibre diameter (0.16 mm) and *l* is the embedded length at each side of the polypropylene sheet (6.5 mm).

The pullout energy was regarded as the mechanical work consumed during the fibre pullout, which was calculated with Eq. (2) through the integration of the area under the load-crack opening curve. The pullout energy was estimated for crack openings of 0.5 mm ($E_{0.5}$) and 2.5 mm ($E_{2.5}$), associated to the serviceability limit state and ultimate serviceability limit state, respectively [47]. Notice that such crack openings are usually defined for conventional fibre reinforced concrete, not UHPFRC. In UHPFRC, a bigger number of cracks tend to appear due to the hardening behaviour of the material. Consequently, a smaller crack opening is expected to occur both in the ultimate limit state for the same strain level.

$$\tau_{max} = \frac{P_{max}}{n.\pi.d.l} \quad \text{Eq. (1)}$$

$$E_w = \int_0^w P_{(w)} dw \quad \text{Eq. (2)}$$

All parameters derived from the pullout test represent the average of 6 determinations per type of fibre. To identify changes induced by the treatment, the surfaces of the fibres were analysed before they were embedded in the UHPFRC matrix and after the pullout tests by means of Scanning Electron Microscopy with X-ray microanalysis (SEM/EDS). Furthermore, to evaluate the fibre-matrix interface, samples of 5x5x5 mm were cut out of the pullout specimens. These samples were dry-polished in a rotary polisher during 10 min at 1000 rpm with a 3 µm grain sandpaper and inspected by SEM/EDS. These analyses were performed in a microscope at the voltage of 15 kV to obtain backscattered electron images.

3 RESULTS AND ANALYSIS

3.1 PULLOUT BEHAVIOR

Fig. 4 shows the average curves that relate the pullout load (P) and the crack opening (w) measured during the pullout test of samples containing untreated fibres and those with

different concentrations of TEOS. All curves reveal a similar behaviour characterized by an initial stage with a significant increase in *P,* with almost no increase in *w*.

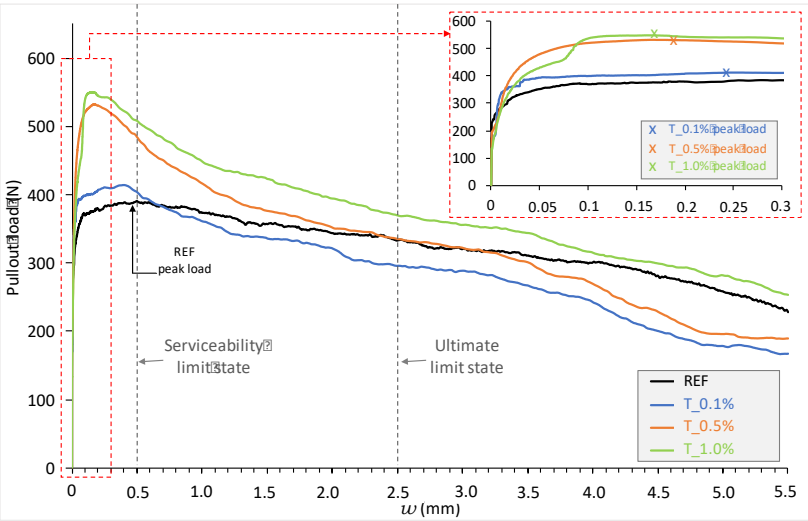

Fig. 4 - Pullout curves.

Debonding initiates for a pullout load around 200 N, being characterized by an increase of both *w* and *P*. Although no clear trend related to the content of TEOS is identified, REF series (untreated) debonding initiates at a load 31.7% bigger than the average registered for series with treated fibres. Despite that, the pullout load reached during the debonding stage in series with treated fibres is up to 35.6% bigger than the observed in REF series. This suggests that the functionalization with TEOS enhances the capability of the fibre-matrix interface to transmit stresses before significant damage appears.

Once *w* reaches approximately 0.04 mm, debonding is completed and fibre slippage takes place. At this stage, the pullout load remains practically constant whereas w increases. From a certain point on, a decrease in P is observed as w increases and the embedded length of the fibres in the matrix is reduced. The decrease registered for the series with TEOS is proportionally bigger than the one verified for the REF series. The bigger load mobilized in the debonding stage of mixes with treated fibres due to a stronger fibre-matrix interface leads to a

more pronounced loss of load capacity. As the interface is debilitated, the pullout load becomes a consequence of frictional forces during the slipping stage.

Elements made with UHPFRC tend to present multiple cracking due to the strain hardening behaviour of the material, which is consistent with the small fibre length normally used. Crack openings of less than 1 mm are expected for both serviceability and ultimate limit states. Therefore, if further statistical analysis confirms that the average differences observed in Fig. 4.; UHPFRC made with treated fibres should outperform those made with reference untreated fibres, since for small crack openings the latter presents higher pullout loads than the former.

3.2 BOND STRENGTH

Fig. 5 in the principal axis shows the maximum bond strength (τ_{max}) calculated from the pullout test results according to Eq. 1. Fig. 5 in the secondary axis shows the average crack opening (w_p) corresponding to τ_{max}. The error bars depict the confidence interval for a significance level of 0.05. The coefficient of variation (CV) of the maximum bond strength and the toughness remains between 8% and 10%. The CV of the load increases with the crack opening, reaching values of 25% for a crack opening of 5.5%. These results are consistent with the findings by [10], [48] and [49]. The τ_{max} of the untreated sample (REF) is comparable to values found in previous studies [10,50], while the τ_{max} of series treated with 0.1%, 0.5% and 1.0% of TEOS were respectively 7.5%, 30.4%, and 35.6% bigger on the average.

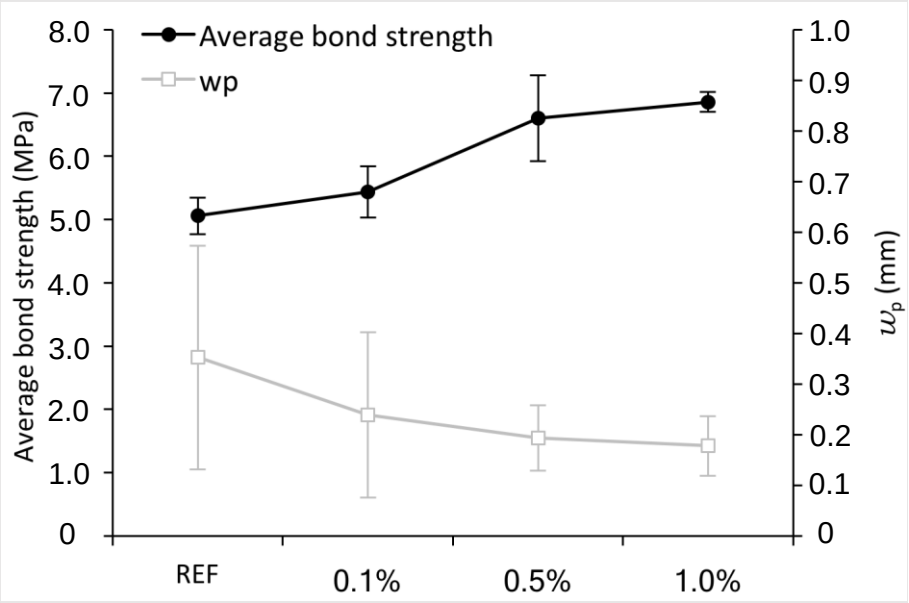

Fig. 5 - Effect of TEOS content in maximum bond strength and in the corresponding crack opening

A one-way ANOVA was conducted to compare the effect of the treatment on τ_{max} and the Duncan's test was used to compare the means. The increase in τ_{max} observed in treated samples in comparison with untreated ones is statistically significant (F=14.47; p-value=0.00). This confirms that the fibre functionalization conducted in this study contributes to enhancing the strength of the fibre-matrix interface.

The post hoc comparison of REF series and series treated with 0.10% of TEOS indicates no significant difference. Conversely, the comparison between the REF series with series treated either with 0.5% of TEOS or with 1.0% of TEOS indicates statistically significant differences. These results reveal that a minimum content of TEOS is required to achieve improvement in the bond strength. Interestingly, no statistically significant difference was found in the comparison between series treated with 0.5% and 1.0% of TEOS. This suggests a saturation effect as no significant differences are observed despite doubling the TEOS concentration. Such observations are consistent with the study conducted by Benzerzour *et al.* [29] that observed optimal results for 0.5% of silane content in the treatment of unsaturated polyester/glass fibre.

A reduction in w_p is observed in the series with treated fibres in comparison with that found in REF series, which becomes more evident as the content of TEOS in the treatment

increases. In fact, series treated with 0.1%, 0.5% and 1.0% of TEOS show w_p 32.3%, 45.0% and 49.6% smaller than that observed in REF series. This behaviour may arise from the formation of a stiffer fibre-matrix interfacial zone that, despite being capable of transmitting higher loads, loses the bearing capacity as damage appears in the interface and the pullout stress the slipping stage governed by friction.

3.3 PULLOUT ENERGY

Fig. 6 shows the average pullout energy calculated with Eq. 2 for crack openings of 0.5 mm ($E_{0.5}$) and 2.5 mm ($E_{2.5}$). Series treated with 0.1%, 0.5% and 1.0% of TEOS show 7.2%, 33.9% and 36.2% bigger $E_{0.5}$ than the ones obtained in REF series. In terms of $E_{2.5}$, the series treated with 0.5% and 1.0% of TEOS remain higher than the REF series, although differences are reduced to 13.1% and 21.9%, respectively. On the contrary, series treated with 0.1% of TEOS show results 2.8% smaller than the obtained for REF series.

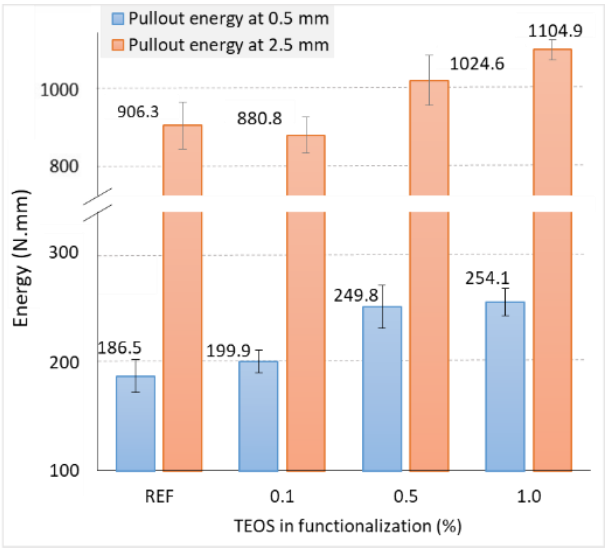

Fig. 6 - Accumulated pullout energy for w_p of 0.5 mm and 2.5 mm

The increase in accumulated pullout energy observed in treated samples in comparison with untreated ones is statistically significant (F=15.45 and p-value=.000 for w_p of 0.5 mm; F=15.877 and p-value=.000 for w_p of 2.5 mm). The direct comparison between REF series and

290 series with 0.1% of TEOS indicate no statistical differences for the crack openings analysed.
291 However, the pullout energy from both series are significantly different from the observed for
292 series treated with 0.5% and 1.0% of TEOS. The difference between series treated with 0.5% and
293 1.0% of TEOS is only statistically significant for w_p of 2.5 mm.

294 These results show that the functionalization of the fibre surface with silane can
295 effectively enhance the fracture toughness of UHPFRC. In the case of UHPFRC, this gain in pullout
296 energy tends to be proportionally bigger for low w_p than for high w_p. As mentioned in section
297 3.2, a minimum silane content is required to achieve significant improvement in the pullout
298 energy. The saturation effect of the silane concentration is not so evident in this case since
299 significant differences in the pullout energy exist between series treated with 0.5% and with
300 1.0% of TEOS for high w_p.

301

302 **4 MICROSTRUCTURAL ANALYSIS**

303 Fig. 7 presents the SEM images of the surfaces of the untreated fibre (Fig. 7.a) and of the
304 fibres treated with TEOS at 0.1%, 0.5% and 1.0% (respectively, Figs.7 b, c, and d), before they
305 were embedded in the UHPFRC specimens. The atomic compositions determined by EDS at the
306 areas highlighted in each figure are also summarized as percentage concentration of each
307 element, placed above each image. Untreated REF fibres have a smooth surface with small
308 scratches formed during the fabrication process. Conversely, the surfaces of treated fibres
309 reveal the formation of a TEOS film that covers the scratches and create deposits that increase
310 the surface roughness of the fibres. The area covered by the deposits increased with the amount
311 of TEOS used in the functionalization. For instance, fibres treated with 0.1% of TEOS display only
312 a few small spots, whereas fibres treated with 1.0% of TEOS have more than 60% of their surface
313 covered by TEOS deposits. The thickness and uniformity of the film seem to increase with the
314 concentrations of TEOS used.

The chemical elements detected by EDS confirm the formation of a film on the surfaces of the treated fibres. Untreated fibres have mainly Fe, Cu, and Zn, which is expected in a brass coated steel fibre. No traces of Si or Ca are observed in this case. In contrast, treated fibres present Si and Ca at their surfaces. The amount of Si at the surface increased as the content of TEOS used for the treatment increased. However, the amount of Ca does not follow the same trend. Si and Ca were the primary components of the deposits observed in the SEM image.

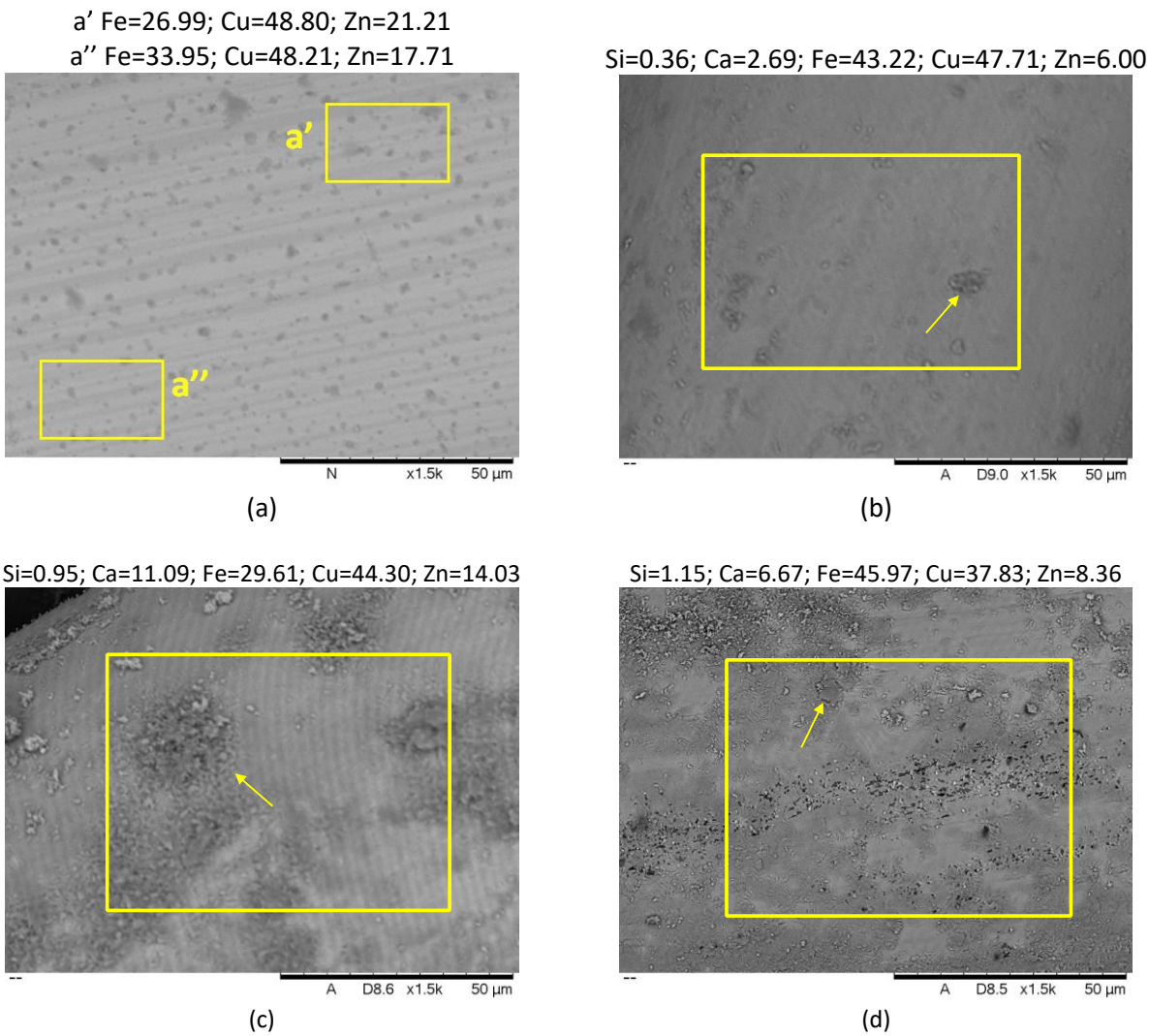

Fig. 7 - SEM images and EDS of fibres before being embedded in the UHPFRC matrix: REF (a), 0.1% (b), 0.5% (c) and 1.0% (d). Yellows arrows indicating typical calcium silicate precipitates.

An in-depth analysis of the reactions expected during the fibre treatment might explain these results. When the silane is dissolved in the solution, the hydrolysis is initiated and the

327 alkoxy groups (Si–OCH_3 or Si–OC_2H_5) are converted to hydroxyl groups (Si–OH), as described in
328 Eq. 3. Subsequently, Si-OH groups and OH^- groups condensate according to Eq. 4 and 5, forming
329 siloxane by covalent bonding [51–53].
330

$$\equiv Si - OR + H_20 \leftrightarrow \equiv Si - OH + ROH \quad \text{Eq. (3)}$$

$$\equiv Si - OR + HO - Si \equiv \leftrightarrow \equiv Si - O - Si \equiv + ROH \quad \text{Eq. (4)}$$

$$\equiv Si - OH + HO - Si \equiv \leftrightarrow \equiv Si - O - Si \equiv + H_2O \quad \text{Eq. (5)}$$

331 Where: R is a radical group (commonly –CH_3 or –C_2H_5).
332

333 After being activated in the NaOH bath, Metal-OH (Me-OH) groups are formed at the
334 surface of the fibres. When these fibres are added into the silane bath, the Me-OH groups react
335 with the hydrolysed silane (eq. 6), forming siloxane chains (eq.7) that are deposited on the
336 surface of the fibres. With the heat treatment, neighbouring silane groups undergo a
337 polycondensation process (eq. 8), forming a film on top of the fibre surface. Then, when the
338 $Ca(OH)_2$ bath is performed, the silane hydroxyls in the silane film react with the calcium
339 hydroxide (eq. 9) to form calcium silicates over the fibres.
340

$$Si(OC_2H_5)_4 + 4H_20 \leftrightarrow\ Si(OH)_4 + 4\ C_2H_6O \quad \text{Eq. (6)}$$

$$Si(OH)_4 + MeOH \leftrightarrow\ MeOSi(OH)_3 + H_2O \quad \text{Eq. (7)}$$

$$MeOSi(OH)_3 + Si(OH)_4 \leftrightarrow\ MeO_2Si_2(OH)_5 + H_2O \quad \text{Eq. (8)}$$

$$MeOSi(OH)_3 + Ca(OH)_2 \leftrightarrow\ MeO_2SiCa(OH)_3 + H_2O \quad \text{Eq. (9)}$$

341 Where: R = –C_2H_5 or –CH_3 and *Me* is the substrate metal oxide
342

343 The heterogeneity of the film thickness varies with the concentration of the silane content
344 in the functionalization solution and with the extent of the hydrolysis/condensation reactions

345 developed during the functionalization process [33]. Solutions with higher concentration of
346 TEOS cause the silane to condensate and form larger siloxane complexes (≡Si-O-Si≡) with
347 neighbouring silanol groups of different lengths. Such molecules may react with the fibre
348 surface, producing a dissimilar thickness of the film on the surface. Another possible explanation
349 relates to heterogeneities in the fibre surface composition. Studies conducted by [33] show that
350 trivalent elements such as Fe^{3+} have a greater possibility of forming crosslinks with hydrolysed
351 silane if compared with surfaces with divalent elements such as Zn^{2+}. Although the concentration
352 of Cu^{2+} is similar in the two regions analysed in Fig. 7.a, the concentration of Fe^{3+} and Zn^{2+} vary
353 from 26% to 36%. This may lead to different silane condensation rates and, consequently, the
354 formation of a film with irregular thicknesses over the surface of the fibres.

355 The silane deposits increase the overall surface in contact with the cementitious matrix
356 and induce more tangential load. Furthermore, deposits might act as anchoring sites that
357 generate inclined forces and affect the damage formation during the pullout. These phenomena
358 may be the physical causes for the enhanced pullout response observed in treated fibres.

359 Fig. 8 presents the morphology of the fibres after the pullout test and the EDS results of
360 the amplified areas. REF fibres (Fig. 8.a) show a smooth surface in which the scratches are more
361 visible than before the pullout test, which may be a result of the friction between fibre and the
362 matrix during the sliding stage of the pullout. A small layer of precipitates is found the surface
363 of REF fibres. The EDS results reveal the presence of Si and Ca, suggesting that the layer is
364 possibly generated by the formation of cement hydration products over the surface.

365 In fibres treated with 0.1% of TEOS (Fig. 8.b), the scratches are less visible than in REF
366 fibres. Moreover, a thicker layer of products remains after the pullout test, although no big
367 deposits are observed. The EDS reveals a higher concentration of Si and Ca than in REF fibres. In
368 fibres treated with 0.5% of TEOS (Fig. 8.c), not only does a layer of hydration products remain
369 over the fibre surface after the pullout test, but also deposits are clearly observed. The
370 concentration of Si and Ca is also slightly bigger than the obtained for the sample treated with

371 0.1% of TEOS. Similar results are obtained for fibres treated with 1.0% of TEOS, with a bigger
372 formation of deposits and a bigger concentration of Si and Ca. In fact, portions of the matrix are
373 observed around the fibre after the pullout test. This confirms that the deposits formed at the
374 surface of the fibre during the treatment enhance the mechanical response, possibly working as
375 anchorage sites that increases the contact between the fibre and the matrix.

376 The comparison of the atomic composition assessed before and after the pullout test for
377 the series show that Si increases from 1% to up to 23%, whereas Ca increases from 11% to 19%.
378 The increase in Si/Ca ratio suggests a densification in the layer originally formed by the
379 treatment over the fibre due to precipitation of the hydration products. Thus, in addition to the
380 physical anchorage effect previously described, a chemical effect could also be responsible for
381 the enhanced pullout performance of the fibres treated with TEOS. The chemical affinity
382 between the silane layer and the formation of hydration products could favour a densification
383 of the interfacial transition zone, leading to a stronger fibre-matrix bond.

384 Although the assessment of durability falls outside the scope of this work, detailed visual
385 inspection of UHPFRC specimens with functionalized and reference fibres showed no evidence
386 of durability problems after the experimental program. Further studies are required to analyse
387 the stability of the functionalization layer and its interaction with the cementitious matrix over
388 a more extended period.

389

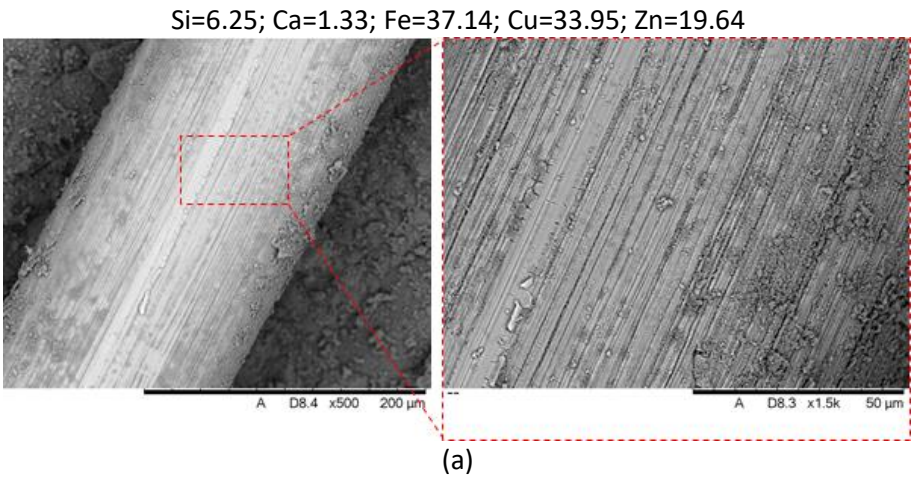

(a)

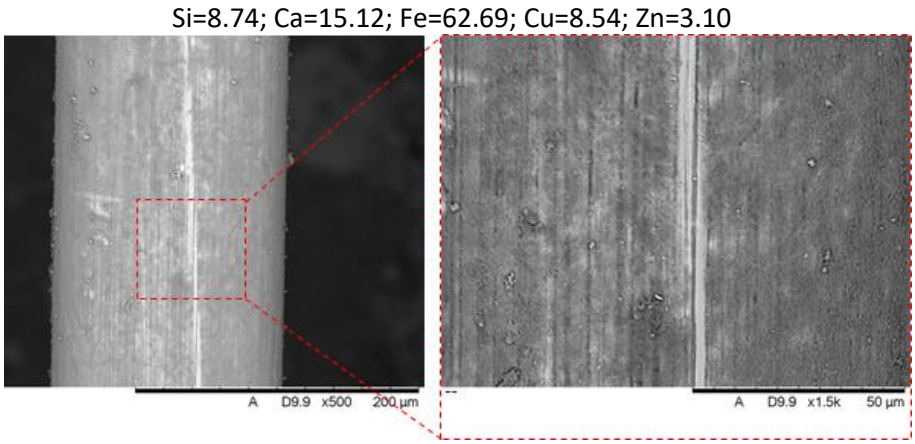

Fig. 8 - SEM images and EDS of fibres after the pullout test: REF (a), 0.1% (b), 0.5% (c) and 1.0% of TEOS (d)

For a more in-depth analysis of the positive effects of the TEOS layer in the fibre-matrix interfacial transition zone, untreated specimens were sliced with a precision saw and the surroundings of the fibres were analysed with SEM. Point and line scanning EDS analysis were

conducted to obtain a profile of composition in relation to the distance from the fibre (see Fig. 9 and Fig. 10). The regions analysed with EDS are indicated by a yellow dot and the line scanning are indicated with a blue line in the corresponding images.

The Si/Ca ratio may be used to indirectly assess the composition of the cementitious matrix [56, 57]. Ratios below 0.3 are characteristic of systems with a high proportion of CH, while ratios bigger than 0.3 indicate systems rich in C-S-H [54]. Studies conducted in systems formed mainly by C-S-H, without CH, indicate a Si/Ca ratio higher than 0.66 [55].

The fibre-matrix interface is dense and homogeneous, with low porosity in all analysed samples, as depicted in Fig. 9.a. REF fibres (Fig. 9.b) present Si/Ca ratios of 0.2 near the fibre. The ratio increases gradually with the distance from the fibre, reaching values consistently above 0.3 at distances bigger than 4 μm. This suggests a preferential CH precipitation around the fibre.

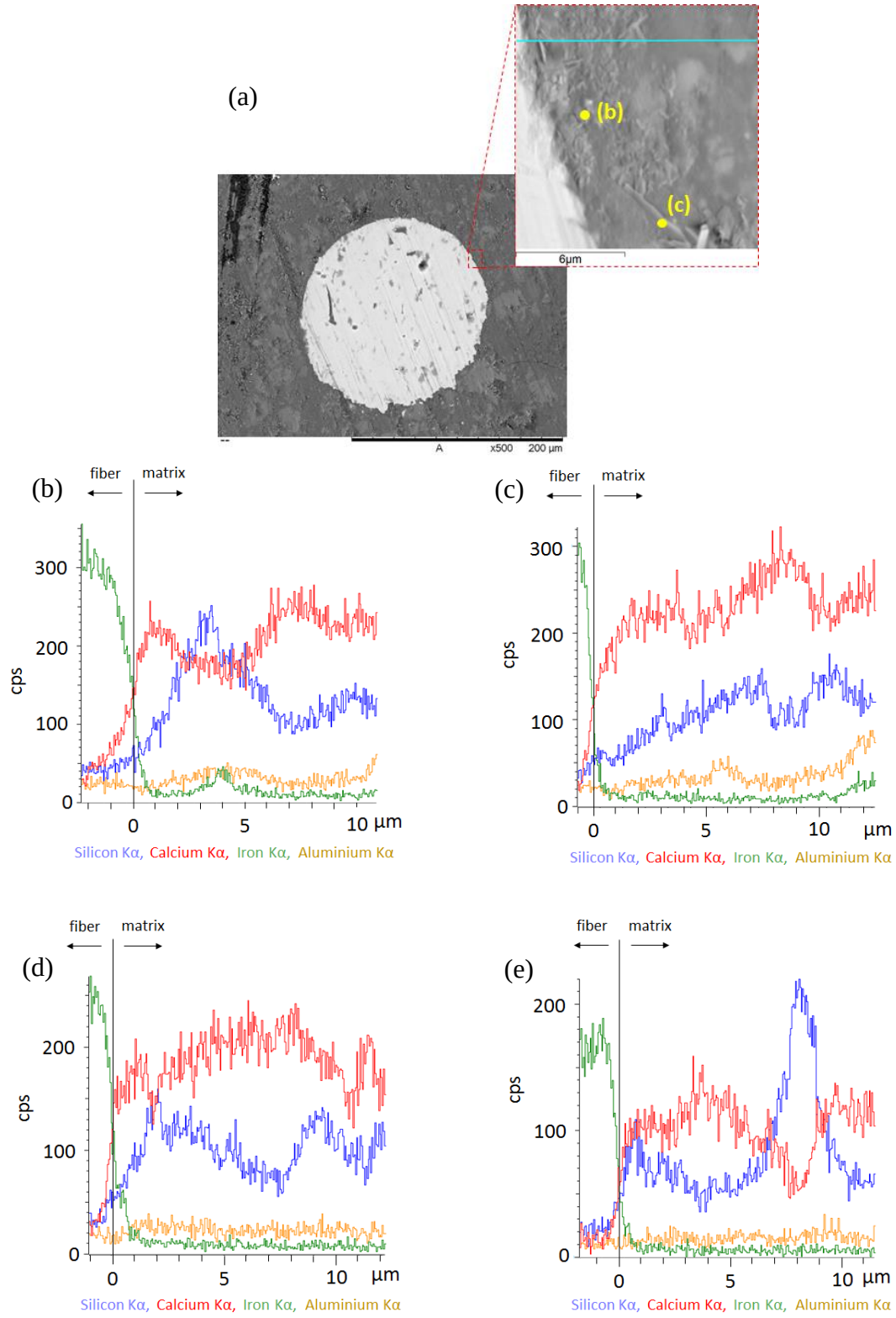

408

409 Fig. 9 - Fibre-matrix cross-section: point and line scan detail (a) and EDS results for series REF

410 (b), with 0.1% (c), with 0.5% (d) and with 1.0% of TEOS (e).

411

In comparison with the REF series, fibres treated with 0.1% of TEOS (Fig. 9.c) show an increase in the Si/Ca in points around the fibre, with values bigger than 0.3. In fact, the Si/Ca reaches 0.3 at a distance of approximately 2 µm from the fibre, in contrast with the 4 µm found for the untreated fibre. This suggests a higher concentration of C-S-H closer to the surface of the fibre treated with TEOS at 0.1%. Analogous results are found for the samples with fibres treated with 0.5% (Fig. 9.d) and with 1.0% (Fig. 9.e) of TEOS. However, in these cases, the Si/Ca ratio of 0.3 is reached at distances even smaller than 1 µm from the fibres. Consequently, the concentration of C-S-H might be higher around the fibres treated with 0.5% and 1.0% than both the untreated fibres and the fibres treated with 0.1% of TEOS.

Interestingly, a more evident peak in the Si counting is observed in samples with treated fibres but not in REF series. This peak is closer to the fibre surface as the content of TEOS in the treatment increases, reaching Si/Ca ratios of approximately 1.0. The series with 0.1%, 0.5% and 1.0% of TEOS show their peaks located, respectively, at 3.5 µm, 2.0 µm and 1.0 µm from the fibre surface (Fig. 10). This suggests a higher level of densification of the interfacial transition zone due to the fibre treatment proposed in this study, confirming the positive chemical interaction caused by the silane film with cement paste.

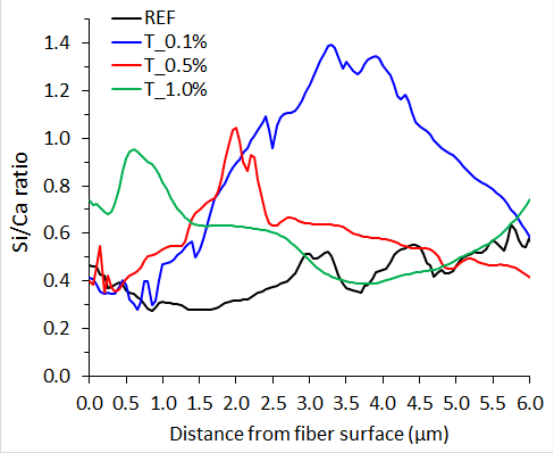

Fig. 10 – Si/ Ca ratio in the transition zone based on EDS line scanning from UHPFRC cross section.

5 CONCEPTUAL MODEL FOR THE FIBRE-MATRIX INTERFACE

Based on the results obtained in this study, a conceptual model of the evolution of fibre-matrix interface is proposed to describe the effect of the functionalization with TEOS adapted from the work by [56]. Fig. 11 depicts the evolution of the hydration of the cement paste and its interaction with the fibre functionalized with TEOS. When the treated fibres come in contact with the cement matrix, the matrix rich in ions (Ca^{2+}, Si^{4+}, and OH^-) reacts with the silane film forming a diffuse layer. This diffuse layer marks a transition between the silane layer and the cement matrix, as shown in Fig. 11.a.

Over time, the alkaline environment around the fibre solubilizes the TEOS film into Si^{4+} and OH^- that reacts with calcium and leads to C-S-H precipitation. This process may consume part of the silane film, increasing the thickness of the diffuse layer, as shown in Fig. 11.b. The C-S-H precipitation reduces the Ca^{2+} availability in the solution around the fibres to form CH. When the Si/Ca ratio is around 0.6, the calcium concentration in the pore solution becomes insufficient to react with the silane film. The increase in C-S-H concentration near the fibre surface could contribute to the densification of the fibre-matrix interface in comparison to the expected in the case of an equivalent non-functionalized fibre.

Differences in the characteristics of these layers may determine how the failure will occur during the pullout test. In case of no functionalization, a low-quality Me-O-Si structure is formed so that the failure may occur at the fibre-silane layer interface or even in the silane layer. The surface of the fibre after the pullout from the matrix should present a morphology similar to that found in untreated fibres.

When functionalization is performed with a small content of silane, a limited amount of Si is available to form and densify the diffuse layer. Consequently, a weak diffuse layer is formed, increasing the likelihood of failure along this faulty layer. Slightly higher pullout loads than those obtained in untreated fibres should be expected. After being pulled out from the matrix, fibres

459 should present a surface covered by a thin layer of silane. This explains the mode of failure
460 observed for the fibres treated with 0.1% of TEOS.

461 In case of proper functionalization with high enough silane content, a good quality diffuse
462 layer is formed. The failure is likely to occur in the cement matrix, leading to bigger surfaces of
463 failure and, hence, bigger pullout loads. Parts of the cementitious matrix remain attached to the
464 surface of the fibre after the he pullout test. This failure mode was observed in fibres treated
465 with 0.5% of TEOS and, more evidently, with 1.0% of TEOS.

466

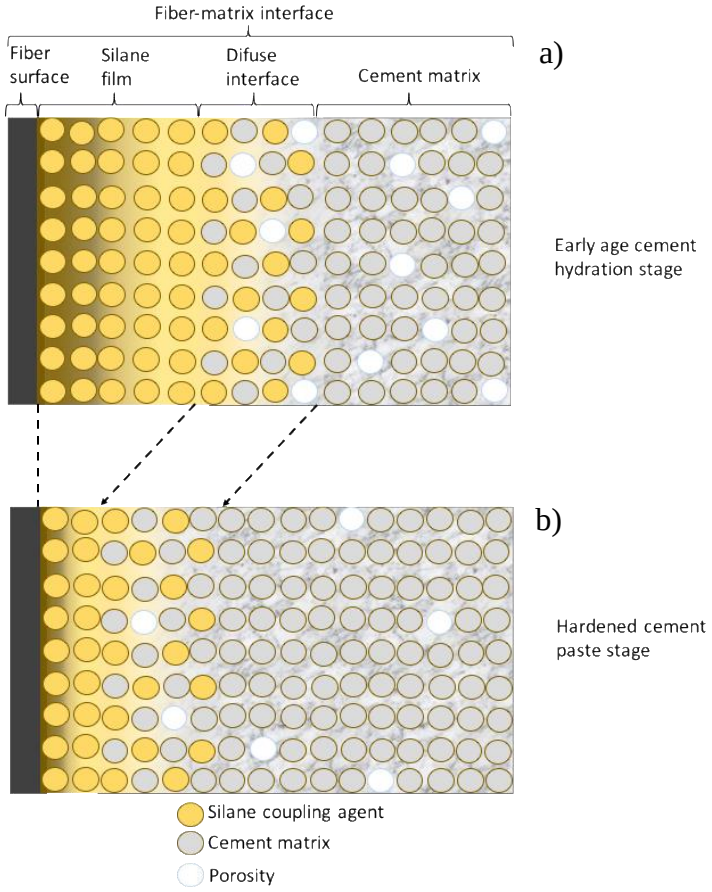

467
468 Fig. 11 - Conceptual model of functionalized fibre-matrix interface at short (a) and long term
469 (b). Adapted from [56]
470

471

472

473

6 CONCLUSIONS

Brass coated steel microfibres were functionalized with TEOS and incorporated in a UHPC matrix. The following conclusions resulted from this study:

- The bond strength measured in the pullout test increase by up to 35.6% in fibres subjected to treatment with TEOS. The energy absorbed for crack openings of 0.5 mm and 2.5 mm were also enhanced for the treated fibres, reaching values up to 36.2% and 21.9% bigger than those of the untreated fibres. Analyses confirm that such differences are statistically significant.
- An optimal content of TEOS should be used to achieve noticeable improvement in the mechanical performance. In this experimental program, a concentration of 0.1% did not produce significant improvements in terms of bond strength and pullout energy in comparison with reference untreated fibres.
- A saturation in the improvement provided by increasing the content of TEOS is also observed. For example, treatments performed with 0.5% and with 1.0% of TEOS lead to almost the same results in terms of bond strength and pullout energy at crack openings of 0.5 mm. Therefore, one of the parameters to be defined in industrial applications is the optimum content of TEOS.
- Evaluations of the morphology and the composition of the fibre-matrix interface reveal that the improvement in performance generated by the treatment relates to physical and chemical changes. The treatment with TEOS increases the roughness of the fibre surface, increasing the total area of contact and, as a result, the pullout force. In fibres treated with a high content of TEOS, silane deposits are formed over the surface of the fibre. These deposits act as mechanical anchorages that generate inclined forces and increase the surface mobilized during the pullout test.

- Results also confirm that a chemical interaction between the silane layer and the cement matrix might also contribute to improve the pullout mechanical performance. The matrix rich in ions (Ca^{2+}, Si^{4+}, and OH^-) react with the silane film forming a diffuse layer. The alkaline environment around the fibre solubilizes the TEOS film into Si^{4+} and OH^- that react with calcium, producing C-S-H in the interface transition zone. EDS measurements reveal that treated fibres show Si/Ca ratios several times higher than untreated fibres, suggesting the additional presence of C-S-H that justifies a stronger interface transition zone.
- A heterogeneity in terms of thickness and area covered by the silane film was observed in the surface of fibres treated with 0.5% and 1.0% of TEOS. This heterogeneity may be attributed to the high concentration of TEOS that tend to condensate and form larger siloxane complexes (≡Si-O-Si≡) with different molecular lengths. Moreover, heterogeneities in the fibre surface composition may favour different silane condensation rates and, consequently, film thicknesses over the fibre's surface.
- The failure mode observed in the pullout test is affected by the treatment applied. Untreated fibres fail in the fibre-matrix interface due to the weaker interface generated. Fibres treated with 0.1% of TEOS do not present enough silane to form a strong diffuse layer around the fibres. Consequently, the failure occurs in the diffuse zone so that a remaining silane layer is observed around the fibre after the pullout test. In contrast, fibres treated with 0.5% and 1.0% of TEOS present a diffuse zone with high concentration of C-S-H and silane deposits that promote a failure through the cement matrix. The inspection of the fibres after the pullout test show the presence of cracked chunks of the matrix around the fibre, confirming the stronger interface transition zone and the need to mobilize a bigger surface during failure. This is the cause of the increment in the pullout load and energy observed.

ACKNOWLEDGMENTS

The authors thank Coordenação de Aperfeiçoamento de Pessoal de Nível Superior (CAPES) by the international scholarship in the project 99999.000243/2015-09, to the Universidad Politècnica de Catalunya (UPC) for providing part of the infrastructure for the research, to the Programa de Pós-graduação em Engenharia Civil (PPGEC) for the fully funded scholarship, to NANOTEC and CERMAT through the LINDEN/UFSC for the technical support in the microstructural investigation, and to Ms. Maria Helena and Dr. Lidiane F. Jochem for their support in the experimental program.

REFERENCES

[1] H.. Bache, Densified cement ultrafine particle-based materials, in: 2nd Int. Conf. Superplast. Concr., Otawa, 1981: p. 33.

[2] J.D. Birchall, A.J. Howard, K. Kendall, Flexural strength and porosity of cements, Nature. 289 (1981) 388–390. doi:10.1038/289388a0.

[3] A.E. Naaman, K. Wille, The path to Ultra-High Performance Fiber Reinforced Concrete (UHP-FRC): Five decades of progress, in: M. Schimidt, E. Fehling, C. Glotzbach, S. Fröhlich, P. S (Eds.), Proc. Hipermat 2012 - 3rd Int. Symp. UHPC Nanotechnol. High Perform. Constr. Mater., Kassel University Press, 2012: pp. 3–16.

[4] H. Russel, G, B.A. Graybeal, Ultra-High Performance Concrete: A State-of-the-Art Report for the Bridge Community - Publication Nº FHWA-HRT-13-060, McLean, 2013. https://www.fhwa.dot.gov/publications/research/infrastructure/structures/hpc/13060/.

[5] K. Kono, H. Musha, T. Kawaguchi, A. Eriguchi, S. Tanaka, T. Kobayashi, M. Ikeda, Durability study of the first PC bridge constructed with ultra high strength fiber reinforced concrete in japan, in: RILEM-Fib-AFGC Int. Symp. Ultra-High Perform. Fibre-Reinforced Concr. UHPFRC 2013, RILEM Publications SARL, Marseille, France, 2013: pp. 239 – 248. http://www.rilem.org/gene/main.php?base=500218&id_publication=422&id_papier=8865 (accessed August 11, 2014).

[6] D.-Y. Yoo, J.-H. Lee, Y.-S. Yoon, Effect of fiber content on mechanical and fracture properties of ultra high performance fiber reinforced cementitious composites, Compos. Struct. 106 (2013) 742–753. doi:10.1016/j.compstruct.2013.07.033.

[7] C. Shi, Z. Wu, J. Xiao, D. Wang, Z. Huang, Z. Fang, A review on ultra high performance concrete: Part I. Raw materials and mixture design, Constr. Build. Mater. 101 (2015) 741–751. doi:10.1016/j.conbuildmat.2015.10.088.

[8] C. DiFrancia, T.C. Ward, R.O. Claus, The single-fibre pull-out test. 1: Review and interpretation, Compos. Part A Appl. Sci. Manuf. 27 (1996) 597–612. doi:10.1016/1359-835X(95)00069-E.

[9] J.M. Alwan, A.E. Naaman, W. Hansen, Pull-out work of steel fibers from cementitious composites: Analytical investigation, Cem. Concr. Compos. 13 (1991) 247–255. doi:10.1016/0958-9465(91)90030-L.

[10] Y.-W. Chan, S.-H. Chu, Effect of silica fume on steel fiber bond characteristics in reactive powder concrete, Cem. Concr. Res. 34 (2004) 1167–1172. doi:10.1016/j.cemconres.2003.12.023.

[11] K. Wille, A.E. Naaman, S. El-Tawil, G.J. Parra-Montesinos, Ultra-high performance concrete and fiber reinforced concrete: achieving strength and ductility without heat curing, Mater. Struct. 45 (2011) 309–324. doi:10.1617/s11527-011-9767-0.

[12] R. Yu, P. Spiesz, H.J.H. Brouwers, Effect of nano-silica on the hydration and microstructure development of Ultra-High Performance Concrete (UHPC) with a low binder amount, Constr. Build. Mater. 65 (2014) 140–150. doi:10.1016/j.conbuildmat.2014.04.063.

[13] S.-T. Kang, J.-K. Kim, Investigation on the flexural behavior of UHPCC considering the effect of fiber orientation distribution, Constr. Build. Mater. 28 (2012) 57–65. doi:10.1016/j.conbuildmat.2011.07.003.

[14] J. Liu, F. Han, G. Cui, Q. Zhang, J. Lv, L. Zhang, Z. Yang, Combined effect of coarse aggregate and fiber on tensile behavior of ultra-high performance concrete, Constr. Build. Mater. 121 (2016) 310–318. doi:10.1016/j.conbuildmat.2016.05.039.

[15] T. Sugama, N. Carciello, L.E. Kukacka, G. Gray, Interface between zinc phosphate-deposited steel fibres and cement paste, J. Mater. Sci. 27 (1992) 2863–2872. doi:10.1007/BF01154093.

[16] P. Frantzis, R. Baggott, Bond between reinforcing steel fibres and magnesium phosphate/calcium aluminate binders, Cem. Concr. Compos. 22 (2000) 187–192. doi:10.1016/S0958-9465(00)00006-8.

[17] D.V. Soulioti, N.-M. Barkoula, F. Koutsianopoulos, N. Charalambakis, T.E. Matikas, The effect of fibre chemical treatment on the steel fibre/cementitious matrix interface, Constr. Build. Mater. 40 (2013) 77–83. doi:10.1016/j.conbuildmat.2012.09.111.

[18] D.G. Aggelis, D.V. Soulioti, E.A. Gatselou, N.-M. Barkoula, T.E. Matikas, Monitoring of the mechanical behavior of concrete with chemically treated steel fibers by acoustic emission, Constr. Build. Mater. 48 (2013) 1255–1260. doi:10.1016/j.conbuildmat.2012.06.066.

[19] E.P. Plueddemann, Silane Coupling Agents, Second, Springer US, Boston, MA, 1991. doi:10.1007/978-1-4899-2070-6.

[20] J. Minet, S. Abramson, B. Bresson, C. Sanchez, V. Montouillout, N. Lequeux, New Layered Calcium Organosilicate Hybrids with Covalently Linked Organic Functionalities, Chem. Mater. 16 (2004) 3955–3962. doi:10.1021/cm034967o.

[21] J. Minet, S. Abramson, B. Bresson, A. Franceschini, H. Van Damme, N. Lequeux, Organic calcium silicate hydrate hybrids: a new approach to cement based nanocomposites, J. Mater. Chem. 16 (2006) 1379. doi:10.1039/b515947d.

[22] A. Franceschini, S. Abramson, V. Mancini, B. Bresson, C. Chassenieux, N. Lequeux, New covalent bonded polymer?calcium silicate hydrate composites, J. Mater. Chem. 17 (2007) 913. doi:10.1039/b613077a.

[23] X.-M. Kong, H. Liu, Z.-B. Lu, D.-M. Wang, The influence of silanes on hydration and strength development of cementitious systems, Cem. Concr. Res. 67 (2015) 168–178. doi:10.1016/j.cemconres.2014.10.008.

[24] J. Cao, D.D.L. Chung, Improving the dispersion of steel fibers in cement mortar by the addition of silane, Cem. Concr. Res. 31 (2001) 309–311. doi:10.1016/S0008-8846(00)00470-1.

[25] G. Collodetti, P.J.P. Gleize, P.J.M. Monteiro, Exploring the potential of siloxane surface modified nano-SiO2 to improve the Portland cement pastes hydration properties, Constr. Build. Mater. 54 (2014) 99–105. doi:10.1016/j.conbuildmat.2013.12.028.

[26] H. Herb, A. Gerdes, G. Brenner-Weiß, Characterization of silane-based hydrophobic admixtures in concrete using TOF-MS, Cem. Concr. Res. 70 (2015) 77–82. doi:10.1016/j.cemconres.2015.01.008.

[27] B. Felekoğlu, A method for improving the early strength of pumice concrete blocks by using alkyl alkoxy silane (AAS), Constr. Build. Mater. 28 (2012) 305–310. doi:10.1016/j.conbuildmat.2011.07.026.

[28] W. Fan, F. Stoffelbach, J. Rieger, L. Regnaud, A. Vichot, B. Bresson, N. Lequeux, A new class of organosilane-modified polycarboxylate superplasticizers with low sulfate sensitivity, Cem. Concr. Res. 42 (2012) 166–172. doi:10.1016/j.cemconres.2011.09.006.
[29] M. Benzerzour, N. Sebaibi, N.E. Abriak, C. Binetruy, Waste fibre–cement matrix bond characteristics improved by using silane-treated fibres, Constr. Build. Mater. 37 (2012) 1–6. doi:10.1016/j.conbuildmat.2012.07.024.
[30] N. Sebaibi, M. Benzerzour, N.E. Abriak, C. Binetruy, Mechanical properties of concrete-reinforced fibres and powders with crushed thermoset composites: The influence of fibre/matrix interaction, Constr. Build. Mater. 29 (2012) 332–338. doi:10.1016/j.conbuildmat.2011.10.026.
[31] Z. Yang, J. Liu, J. Liu, C. Li, H. Zhou, Silica modified synthetic fiber for improving interface property in FRCC, in: J.A.O. Barros (Ed.), 8th RILEM Int. Symp. Fibre Reinf. Concr. Challenges Oppor. (BEFIB 2012), RILEM Publications SARL, 2012: pp. 347–357. http://www.rilem.org/gene/main.php?base=500218&id_publication=419&id_papier=8647.
[32] L. Téllez, F. Rubio, R. Peña-Alonso, J. Rubio, Seguimiento por espectroscopia infrarroja (FT-IR) de la copolimerización de TEOS (tetraetilortosilicato) y PDMS (polidimetilsiloxano) en presencia de tbt (tetrabutiltitanio), Bol. La Soc. Esp. Ceram. y Vidr. 43 (2004) 883–890. doi:10.3989 /cyv.2004.v43.i5.
[33] W.J. Van Ooij, D. Zhu, M. Stacy, A. Seth, T. Mugada, J. Gandhi, P. Puomi, Corrosion Protection Properties of Organofunctional Silanes — An Overview, Tsinghua Sci. Technol. 10 (2005) 639–664.
[34] P.H. Suegama, I. V Aoki, Electrochemical behavior of carbon steel pre-treated with an organo functional bis-silane filled with copper phthalocyanine, J. Braz. Chem. Soc. 19 (2008) 744–754. doi:10.1590/S0103-50532008000400019.
[35] M.R. Bagherzadeh, A. Daneshvar, H. Shariatpanahi, Novel water-based nanosiloxane epoxy coating for corrosion protection of carbon steel, Surf. Coatings Technol. 206 (2012) 2057–2063. doi:10.1016/j.surfcoat.2011.05.036.
[36] W. Yuan, van Ooij WJ, Characterization of Organofunctional Silane Films on Zinc Substrates, J. Colloid Interface Sci. 185 (1997) 197–209. http://www.ncbi.nlm.nih.gov/pubmed/9056330.
[37] A.V. Cunliffe, S. Evans, D.A. Tod, S.A. Torry, P. Wylie, Optimum preparation of silanes for steel pre-treatment, Int. J. Adhes. Adhes. 21 (2001) 287–296. doi:10.1016/S0143-7496(01)00004-5.
[38] R. Yu, P. Spiesz, H.J.H.J.H. Brouwers, Development of an eco-friendly Ultra-High Performance Concrete (UHPC) with efficient cement and mineral admixtures uses, Cem. Concr. Compos. 55 (2015) 383–394. doi:10.1016/j.cemconcomp.2014.09.024.
[39] K. Koh, G.S. Ryu, J. Park, K.H. An, S.W. Kim, Effects of the composing materials on the rheological and mechanical properties of ultra-high performance concrete (UHPC), in: F. Toutlemonde, J. Resplendino (Eds.), RILEM-Fib-AFGC Int. Symp. Ultra-High Perform. Fibre-Reinforced Concr. UHPFRC 2013, RILEM Publications SARL, Marseille, France, 2013: pp. 749–756.
[40] D.J. Kim, S.H. Park, G.S. Ryu, K.T. Koh, Comparative flexural behavior of Hybrid Ultra High Performance Fiber Reinforced Concrete with different macro fibers, Constr. Build. Mater. 25 (2011) 4144–4155. doi:10.1016/j.conbuildmat.2011.04.051.
[41] AENOR, Asociación Española de Normalización y Certificación - UNE-EN 197-1 - Cemento - Parte1: Composición, especificaciones y criterios de conformidad de los cementos comunes, 2011. http://www.aenor.es/aenor/normas/normas/fichanorma.asp?tipo=N&codigo=N0048623#.VyEWb1bhDDd.
[42] ASTM, C1437 - Standard test method for flow of hydraulic cement mortar, 2013.
[43] AENOR, UNE-EN 196-1. Métodos de ensayo de cementos - Parte 1: Determinación de

672 resistencias mecánicas, (2005) 35.
673 [44] Y. Lee, S.-T. Kang, J.-K. Kim, Pullout behavior of inclined steel fiber in an ultra-high
674 strength cementitious matrix, Constr. Build. Mater. 24 (2010) 2030–2041.
675 doi:10.1016/j.conbuildmat.2010.03.009.
676 [45] J.-P. Won, B.-T. Hong, S.-J. Lee, S.J. Choi, Bonding properties of amorphous micro-steel
677 fibre-reinforced cementitious composites, Compos. Struct. 102 (2013) 101–109.
678 doi:10.1016/j.compstruct.2013.02.015.
679 [46] Z. Wu, C. Shi, K.H. Khayat, Influence of silica fume content on microstructure
680 development and bond to steel fiber in ultra-high strength cement-based materials
681 (UHSC), Cem. Concr. Compos. 71 (2016) 97–109.
682 doi:10.1016/j.cemconcomp.2016.05.005.
683 [47] Fedération Internationale du Béton, International Federation for Structural Concrete
684 (fib) Model Code 2010 - First complete draft - Volume 1 - Bulletin 55: march, Lausanne -
685 Switzerland, 2010.
686 [48] S.H. Kang, T.-H. Ahn, D.J. Kim, Effect of grain size on the mechanical properties and
687 crack formation of HPFRCC containing deformed steel fibers, Cem. Concr. Res. 42
688 (2012) 710–720. doi:10.1016/j.cemconres.2012.02.011.
689 [49] S.H. Kang, J.J. Kim, D.J. Kim, Y.-S. Chung, Effect of sand grain size and sand-to-cement
690 ratio on the interfacial bond strength of steel fibers embedded in mortars, Constr.
691 Build. Mater. 47 (2013) 1421–1430. doi:10.1016/j.conbuildmat.2013.06.064.
692 [50] Z. Wu, K.H. Khayat, C. Shi, Effect of nano-SiO 2 particles and curing time on
693 development of fiber-matrix bond properties and microstructure of ultra-high strength
694 concrete, Cem. Concr. Res. 95 (2017) 247–256. doi:10.1016/j.cemconres.2017.02.031.
695 [51] C.J. Brinker, Hydrolysis and condensation of silicates: Effects on structure, J. Non. Cryst.
696 Solids. 100 (1988) 31–50. doi:10.1016/0022-3093(88)90005-1.
697 [52] J.C. Ro, I.J. Chung, Sol-gel kinetics of tetraethylorthosilicate (TEOS) in acid catalyst, J.
698 Non. Cryst. Solids. 110 (1989) 26–32. doi:10.1016/0022-3093(89)90178-6.
699 [53] Y. Hui, D. Zishang, J. Zhonghua, X. Xiaoping, Sol-gel process kinetics for Si(OEt)4, J. Non.
700 Cryst. Solids. 112 (1989) 449–453. doi:10.1016/0022-3093(89)90571-1.
701 [54] R.P. Salvador, S.H.P. Cavalaro, I. Segura, A.D. De, Early age hydration of cement pastes
702 with different types of accelerators for sprayed concrete, Constr. Build. Mater. 111
703 (2016) 1–29. doi:10.1016/j.conbuildmat.2016.02.101.
704 [55] A. Nonat, The structure and stoichiometry of C-S-H, Cem. Concr. Res. 34 (2004) 1521–
705 1528. doi:10.1016/j.cemconres.2004.04.035.
706 [56] T. Materne, F. Buyl, G.L. Witucki, Organosilane Technology in Coating Applications:
707 Review and Perspectives, Dow Corning. (2010) 1–16.
708